scientific data

Check for updates

OPEN

DATA DESCRIPTOR

The University of California San Diego Post-Treatment Glioblastoma (UCSD-PTGBM) annotated multimodal MRI Dataset

Louis Gagnon[1,2]✉, Diviya Gupta[1,3], Uyen Nguyen[1], Maria Correia de Verdier[1,4], Rachit Saluja[5,6], George Mastorakos[7], Nathan White[7], Vanessa Goodwill[8], Carrie R. McDonald[9], Thomas Beaumont[10], Christopher Conlin[1], Tyler M. Seibert[1,9,11], Jona Hattangadi-Gluth[9], Santosh Kesari[12], Jessica D. Schulte[13], David Piccioni[13], Kathleen M. Schmainda[14], Nikdokht Farid[1], Anders M. Dale[1,13] & Jeffrey D. Rudie[1]

We present the University of California San Diego post-treatment glioblastoma (UCSD-PTGBM) annotated multimodal MRI dataset. The UCSD-PTGBM dataset includes 243 timepoints on 178 subjects with histopathologically-proven glioblastoma who were imaged with an advanced brain tumor protocol on 3 Tesla MRI scanners. Sequences include standard 3D imaging, as well as multishell diffusion (Restricted Spectrum Imaging, RSI) and perfusion imaging techniques (Arterial Spin Labelling, ASL and Dynamic Susceptibility Contrast, DSC), and neuroradiologist approved voxelwise tumor segmentations for both traditional segmentation masks and cellular tumor segmentations. The dataset also includes isocitrate dehydrogenase (IDH) mutation status and O6-methylguianine-DNA methyl-transferase (MGMT) promotor methylation status, as well as overall survival and progression free survival information for a subset of cases. We hope that researchers around the world will use these data to continue to improve analysis of post-operative MRI on glioblastoma patients, translate their findings into clinical practice and improve the management and outcome for these patients.

Background & Summary

Glioblastoma (GBM) is the most common primary malignant brain tumor in the adult population[1] and has a very poor prognosis with a median overall survival (OS) of 15–21 months and a 5-year OS of 10%[2]. Treatment for glioblastoma involves a multi-modal approach tailored to the tumor's characteristics and the patient's functional status and includes surgery, radiation therapy, and systemic therapies (i.e. chemotherapy, immunotherapy, and targeted therapy). Multimodal MRI is used for evaluating tumor burden, surgical planning, and monitoring disease response to treatment both before and after surgery. Post-treatment imaging of glioblastoma is a fundamental part of patient management that significantly influences clinical decision making and outcomes. The combination of treatment-related changes, including resection cavities, blood products,

[1]Department of Radiology, University of California San Diego, San Diego, USA. [2]Department of Radiology and Nuclear Medicine, Laval University, Québec, Canada. [3]Department of Radiology, University of California Los Angeles, Los Angeles, USA. [4]Department of Surgical Sciences, section of Neuroradiology, Uppsala University, Uppsala, Sweden. [5]Department of Electrical and Computer Engineering, Cornell University and Cornell Tech, New York, NY, USA. [6]Department of Radiology, Weill Cornell Medicine, New York, USA. [7]Cortechs.ai, San Diego, USA. [8]Department of Pathology, University of California San Diego, San Diego, USA. [9]Department of Radiation Medicine and Applied Sciences, University of California San Diego, San Diego, USA. [10]Department of Neurosurgical Surgery, University of California San Diego, San Diego, USA. [11]Department of Bioengineering, University of California San Diego, San Diego, USA. [12]Department of Translational Neurosciences, Pacific Neuroscience Institute and Saint John's Cancer Institute at Providence Saint Johns' Health Center, Santa Monica, CA, USA. [13]Department of Neuroscience, University of California San Diego, San Diego, USA. [14]Department of Biophysics, Medical College of Wisconsin, Milwaukee, Wisconsin, USA. ✉e-mail: louis.gagnon.9@ulaval.ca

	Total	Survival Analysis subset
Demographics		
Timepoints	243	94
Patients	178	94
Age (years)	56 ± 13	58 ± 13
Male	116 (65%)	67 (71%)
Female	62 (35%)	27 (29%)
GTR+	87 (49%)	38 (40%)
MGMT+	76/149 (51%)	17/61 (28%)
MGMT−	73/149 (49%)	44/61 (72%)

Table 1. Patient Demographics. Note. Data presented as mean ± standard deviation or number (percentage). GTR = gross total resection, MGMT = O^6-methylguanine-DNA methyl-transferase promoter methylation.

post-radiation inflammation, and gliosis, combined with the baseline ill-defined tumor borders seen in glioblastomas makes the radiological assessment of post-surgical MRI challenging[3]. Differentiating recurrent disease from post-treatment changes is crucial, since a delay in the diagnosis of tumor recurrence and progression may prevent prompt treatment, while overcalling recurrent tumor may result in unnecessary interventions. Nevertheless, this task remains a challenge even for experienced neuroradiologists.

Over the last 15 years, Machine Learning has opened the door for automated tumor segmentation tools[4]. In parallel, radiomics[5] has been applied to outcome-related tasks such as overall survival prediction[6,7], radiogenomics[8], and differentiating pseudoprogression[9] from progression based on MRI[10,11]. These models use annotated data that need to be corrected and approved by a radiologist. Most prior research on brain tumor segmentation has been performed in the pre-treatment setting, with a recent survey finding that 98.3% of published glioma segmentation studies had been performed on pre-operative imaging[12]. While several recent studies involving glioma segmentation have been performed in the post-treatment setting[13–21], relatively little post-treatment glioma data with voxelwise annotations exists publicly[21–24].

Here we present the University of California San Diego post-treatment glioblastoma (UCSD-PTGBM) annotated multimodal MRI dataset. We aim to provide researchers around the world with a multimodal MRI dataset collected on post-operative glioblastoma patients, and annotated by neuroradiologist. Moreover, our dataset includes advanced imaging such as multishell high b-value diffusion MRI (Restricted Spectrum Imaging, RSI), Arterial Spin Labelling (ASL) perfusion, and Dynamic Susceptibility Contrast (DSC) perfusion sequences. The dataset also includes clinical information such as isocitrate dehydrogenase (IDH) mutation status and O6-methylguianine-DNA methyl-transferase (MGMT) promotor methylation status, as well as overall survival and progression free survival information for a subset of cases. We hope that this dataset will help researchers to improve analysis of post-operative MRI on glioblastoma patients, which could lead to improvement in the management and outcome for these patients.

Methods

Patient population and demographic data. This retrospective study was approved by the institutional review board of the University of California San Diego (IRB #809620) and the requirement for informed consent was waived since a significant fraction of the patients had passed away. Data were de-identified and collected according to the Health Insurance Portability and Accountability Act (HIPAA) standard. Only (LG, first author) had control of inclusion of any data and information that might present a conflict of interest. The dataset presented here is the same dataset used in our previous work on cellular tumor segmentation[7]. A subset of this dataset (only the T1 pre-contrast, T1 post-contrast, T2 and fluid attenuated inversion recovery (FLAIR) sequences) was also used in the BraTS 2024 dataset[23]. Patients diagnosed with glioblastoma from January 2010 to June 2022 at UCSD were identified from chart review of the institutional medical record. A drawback of our dataset is the unique institutional origin (UCSD) of all cases, which limits the diversity of imaging protocol and populations. Inclusion criteria included post-treatment MRI with the multishell diffusion sequence RSI. The pathology database was searched to enrich the sample for cases with pathology proven progression and treatment-related changes. 244 unique patients (315 timepoints) were initially identified, but 54 timepoints were rejected due to missing MRI sequences and 18 timepoints were rejected due to inability to distinguish treatment-related changes from residual/recurrent tumor with confidence. The final dataset consisted of 178 patients (243 timepoints) with mean age 56 + /- 13 years [std], 121 men. Data has subject-level identifiers to avoid data leakage. 192 timepoints had residual or recurrent tumor (45 pathology proven), while the remaining 51 timepoints had only post treatment changes (including 4 pathology-proven pseudoprogression (PsP), 9 clinically confirmed PsP, 10 clinically confirmed radiation necrosis, and 28 non-specific post-treatment changes). Overall survival (OS) and progression free survival (PFS) information is available for a subset of 94 patients (58 + /- 13 years, 67 men) with an MRI scan with RSI within 90 days following surgery. IDH mutation status is available for 168 timepoints. MGMT methylation status is available for 149 timepoints. An overview of patient demographics is presented in Table 1.

Imaging data. An example from the dataset is presented in Fig. 1. Imaging protocol included pre- and postgadolinium 3D volumetric T1-weighted inversion recovery spoiled gradient-recalled sequences (TE/TR = 2.8/6.5 ms, TI = 450 ms, flip angle = 8 °, FOV = 24 cm, matrix = 0.93 × 0.93 × 1.2 mm), a 3D T2- weighted FLAIR sequence (TE/TR = 126/6000 ms, TI = 1863 ms, FOV = 24 cm, matrix = 0.93 × 0.93 × 1.2 mm), a

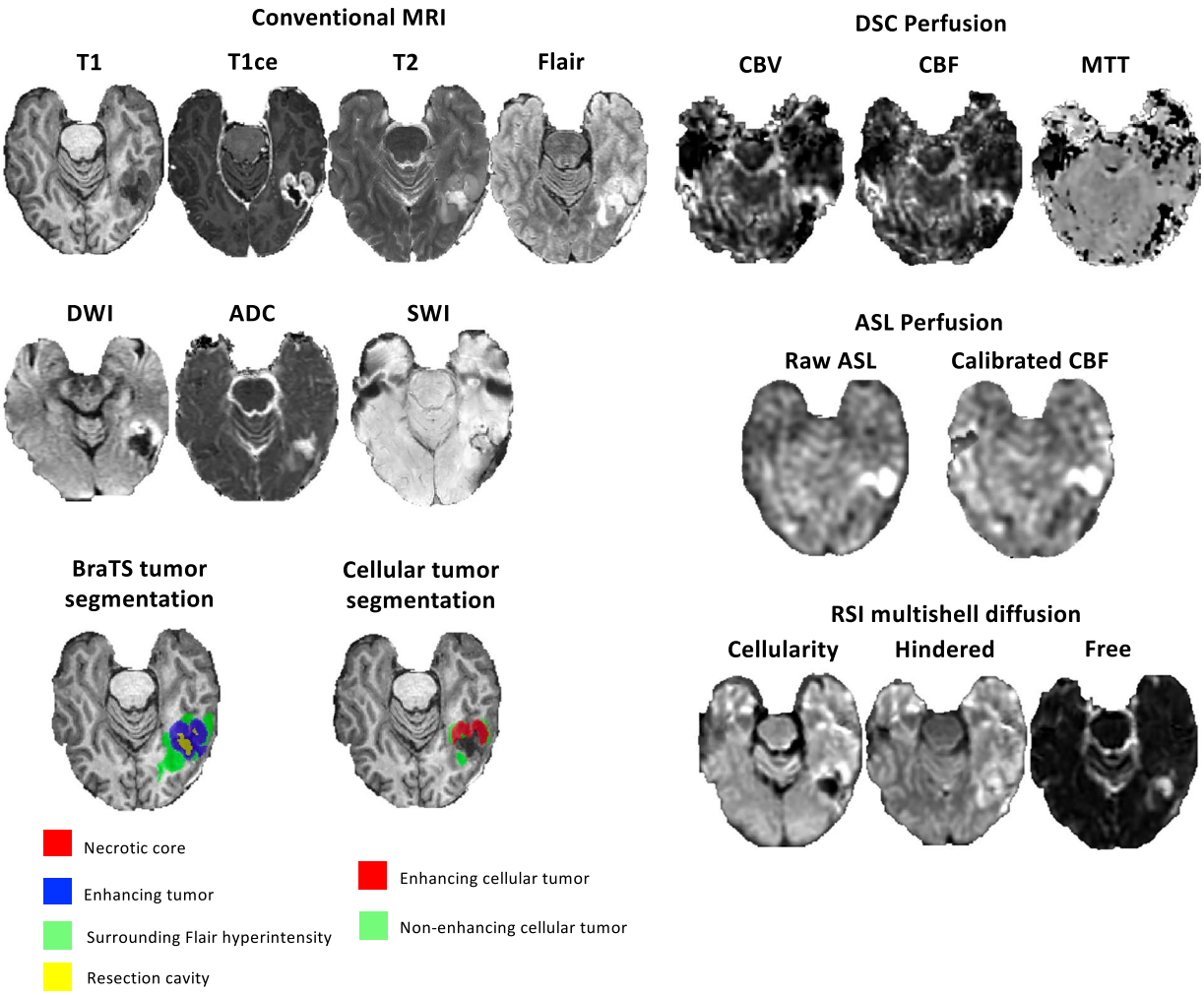

Fig. 1 Dataset available MRI sequences and annotations. T1 = T1 pre-contrast, T1ce = T1 contrast-enhanced, FLAIR = Fluid attenuated inversion recovery, DWI = Diffusion-Weighted Imaging, ADC = Apparent Diffusion Coefficient, SWI = Susceptibility-Weighted Imaging, DSC = Dynamic Susceptibility Contrast, CBV = Cerebral Blood Volume, CBF = Cerebral Blood Flow, MTT = Mean Transit Time, ASL = Arterial Spin Labelling, RSI = Restricted Spectrum Imaging.

T2-weighted sequence (TE/TR = 81.8/5276 ms, 0.47 × 0.47 mm, slice thickness = 3 mm), a susceptibility-weighted sequence (TE/TR = 28/47 ms, 0.47 × 0.47 mm, slice thickness = 3 mm) and a diffusion-weighted sequence (TE/TR = 82/9500 ms, 0.93 × 0.93 mm, slice thickness = 3 mm). For RSI, a single-shot pulsed-field gradient spin-echo echo-planar imaging sequence was used (TE/TR 1⁄4 96 ms/17 s; FOV 1⁄4 24 cm, matrix = 128 × 128 × 48; slice thickness = 2.5 mm) with 4 b-values (b = 0, 500, 1500, and 4000 s/mm2), and 6, 6, and 15 unique diffusion directions for each nonzero b-value, respectively (28 total volumes, ~8 min scan time). DSC perfusion MRI was performed using a gradient-echo echo-planar-imaging (EPI) sequence (TE/TR = 35/1600 ms; FA = 90°; slice thickness 5 mm with intersection gap of 1 mm; 22 axial slices; FOV = 25 cm; matrix = 96 × 96) 0.1 mmol/kg of gadobenate dimeglumine (Bracco Diagnostics) or gadobutrol (Bayer AG), was injected intravenously with an MR-compatible power injector at a rate of 2–3 mL/s through an antecubital angiocatheter, followed immediately by a 20-mL continuous saline flush. The multi-section image set was acquired every 1–2 s during the first pass of the contrast agent until 60 time points were obtained. Aterial Spin Lageling (ASL) with a pseudo-continuous scheme (pCASL) was acquired using the standard GE protocol with in-line analysis. All patients were scanned on 3 T clinical scanners (GE Signa Excite HDx and GE Discovery MR750 with 8-channel head coil) at two different institutions affiliated with UCSD.

Image pre-processing. The RSI images were processed using a standard processing pipeline described in White *et al.*[25] to derive cellularity maps. The diffusion signal in each voxel was fit by using a linear mixture model of restricted and hindered water compartments with spheric and cylindric geometries. The resulting spherically restricted water fraction formed the basis of our RSI cellularity maps. To maximize sensitivity and specificity to the spherically restricted water fraction, a beam-forming filter was applied to our cellularity maps to reduce residual signal contamination from cylindrically restricted and hindered water compartments. DSC images were processed using the Matlab DSC toolbox[26] to compute Cerebral Blood Volume (CBV) using a leakage correction

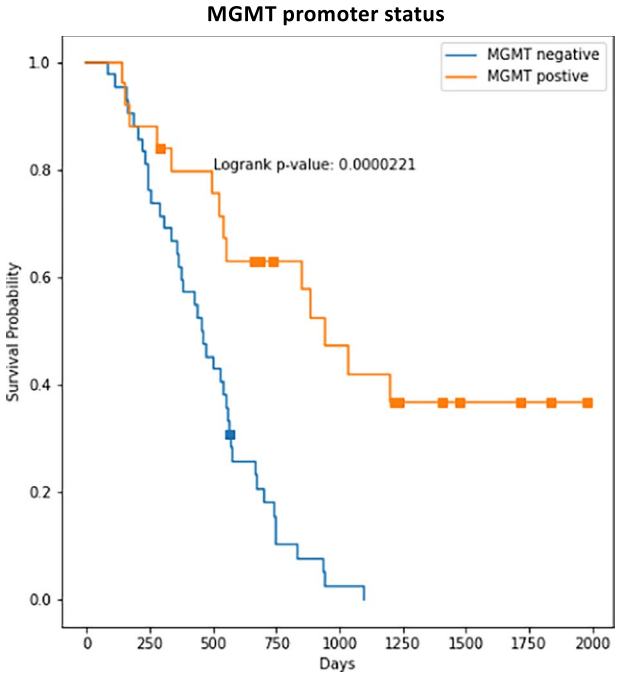

Fig. 2 Kaplan-Meier curves for MGMT methylated and unmethylated groups. As expected, patients with MGMT methylation have a significant higher median survival ($p = 0.00002$).

algorithm[27]. Images from all modalities were registered and resampled to a 256x256x256 1 mm isotropic resolution MNI brain atlas[28]. A brain mask was obtained from the FLAIR images using an in-house custom nnUNet skull stripping network and was subsequently applied to the other modalities.

All pre-processing steps were manually reviewed by a neuroradiology fellow (author L.G.) to ensure proper co-registration. Any registration errors were manually corrected before inclusion in the dataset. All the conventional and RSI data were manually reviewed by an attending radiologist during the cellular tumor segmentation procedure (J.D.R.). All the DSC and ASL processed data were manually reviewed (L.G.) and re-processed manually in few cases to ensure good quality.

Tumor segmentation. *Standard BraTS segmentation.* Multicompartment tumor segmentation was done using the BraTS challenge standard annotation[4]. Image first underwent automated segmentation by a Deep Learning software (OnQ^{TM} Neuro, Cortechs.ai, San Diego). Segmentations were then manually corrected by trained radiologists. Segmentation included four major tumor compartments: enhancing tumor, non-enhancing/necrotic tumor core, surrounding non-enhancing FLAIR hyperintensity, and resection cavity. All manually corrected BraTS-type (enhancing tumor, necrotic core, surgical cavity, FLAIR signal surrounding hyperintensity) tumor segmentations were then reviewed by a board-certified neuroradiologist "approver" (authors J.D.R. and L.G.) in line with the established annotator/approval model used in the BraTS challenges[4,23,29]. In cases where the approver identified an inaccurate or incomplete segmentation, the case was returned to a different annotator for further refinement with notes indicating remaining issues. This process was repeated, if necessary, until the approver judged that the segmentation was accurate. As such, the inter-annotator variability could not be assessed and no cross-validation was performed.

Cellular tumor segmentation. For each patient, cellular tumor was manually segmented by an attending neuroradiologist with three years of experience post fellowship and extensive segmentation experience (J.D.R.), as well as a neuroradiology fellow (L.G.). Segmentations were performed based on all available clinical, pathological and imaging history including a thorough review of prior and subsequent MRIs. All cases with post-treatment changes (pseudoprogression, radiation necrosis, and post-treatment changes only) were reviewed by a third neuroradiologist with 13 years of experience post fellowship (N.F.). The neuroradiologists manually segmented total cellular tumor (TCT), representing both enhancing and nonenhancing cellular tumor, while the ground truth enhancing cellular tumor (ECT) was extracted by masking the manual segmentation with the conventional enhancing tumor mask generated as described in the previous section. The non-enhancing cellular tumor (NECT) mask was obtained by masking out ECT from TCT.

Data Records

This dataset is available through The Cancer Imaging Archive (TCIA)[30] under a CC BY 4.0 license. The material ca be copied and redistributed in any medium or format for any purpose, even commercially. It is to note that 40 patients (60 timepoints) are held out for the 2025 BraTS challenge and will be released in early 2026. MRI images and tumor segmentations are stored in The Neuroimaging Informatics Technology Initiative (NIfTI) format.

Clinical information is stored in a comma-separated values (.CSV) file. Data has subject-level identifiers to avoid data leakage. Data includes T1-pre and post contrast, T2, FLAIR, diffusion-weighted imaging (DWI) and apparent diffusion coefficient (ADC), susceptibility-weighted imaging (SWI), Arterial Spin Labeling (ASL) and corresponding calibrated cerebral-blood-flow (CBF) maps, Dynamic susceptibility contrast (DCS) perfusion imaging (CBV, CBF and mean-transit-time), Restricted Spectrum Imaging (cellularity, hindered, free water).

Technical Validation

MGMT promoter stratification. To demonstrate the internal consistency of our data, we computed the Kaplan-Meier curves for our patient cohort stratified by the MGMT promoter status. Results are shown in Fig. 2. A significant higher ($p = 0.00002$) median survival time for patients with methylated MGMT status is observed, which is consistent with the literature[31,32].

Data availability

This dataset is available through The Cancer Imaging Archive (TCIA)[30] under a CC BY 4.0 license (https://www.cancerimagingarchive.net/collection/ucsd-ptgbm/).

Code availability

The code use to co-register and pre-process the data is available at https://github.com/rachitsaluja/UCSF-ALPTDG-benchmarks15. The code used to process the DSC data is publicly available as part of the Matlab DSC toolbox[26].

Received: 31 March 2025; Accepted: 18 December 2025;
Published online: 06 January 2026

References

1. Louis, D. N. *et al.* The 2021 WHO Classification of Tumors of the Central Nervous System: a summary. *Neuro-oncology.* **23**(8), 1231–1251, https://doi.org/10.1093/neuonc/noab106 (2021).
2. Gutman, D. A. *et al.* MR Imaging Predictors of Molecular Profile and Survival: Multi-institutional Study of the TCGA Glioblastoma Data Set. *Radiology.* **267**(2), 560–569, https://doi.org/10.1148/radiol.13120118 (2013).
3. Taylor, C., Ekert, J. O., Sefcikova, V., Fersht, N. & Samandouras, G. Discriminators of pseudoprogression and true progression in high-grade gliomas: A systematic review and meta-analysis. *Sci Rep-uk.* **12**(1), 13258, https://doi.org/10.1038/s41598-022-16726-x (2022).
4. Baid, U. *et al.* The RSNA-ASNR-MICCAI BraTS 2021 Benchmark on Brain Tumor Segmentation and Radiogenomic Classification. *arXiv*. https://doi.org/10.48550/arxiv.2107.02314 (2021).
5. Lambin, P. *et al.* Radiomics: Extracting more information from medical images using advanced feature analysis. *Eur J Cancer.* **48**(4), 441–446, https://doi.org/10.1016/j.ejca.2011.11.036 (2012).
6. Bakas, S. *et al.* Identifying the Best Machine Learning Algorithms for Brain Tumor Segmentation, Progression Assessment, and Overall Survival Prediction in the BRATS Challenge. *arXiv*. https://doi.org/10.48550/arxiv.1811.02629 (2018).
7. Gagnon, L. *et al.* Deep Learning Segmentation of Infiltrative and Enhancing Cellular Tumor at Pre- and Posttreatment Multishell Diffusion MRI of Glioblastoma. *Radiol Artif Intell.* **6**(5), e230489, https://doi.org/10.1148/ryai.230489 (2024).
8. Ellingson, B. M. Radiogenomics and Imaging Phenotypes in Glioblastoma: Novel Observations and Correlation with Molecular Characteristics. *Curr Neurol Neurosci Rep.* **15**(1), 506, https://doi.org/10.1007/s11910-014-0506-0 (2014).
9. Abrol, S. *et al.* Radiomic analysis of pseudo-progression compared to true progression in glioblastoma patients: A large-scale multi-institutional study. *J Clin Oncol.* **35**(15_suppl), 2015–2015, https://doi.org/10.1200/jco.2017.35.15_suppl.2015 (2017).
10. Suter, Y. *et al* Machine Learning in Clinical Neuroimaging and Radiogenomics in Neuro-oncology. *Lect Notes Comput Sci.* 129–138, https://doi.org/10.1007/978-3-030-66843-3_13 (2020).
11. Gagnon, L. *et al.* Comparing DSC-CBV, DSC-CBF and ASL for Detecting Residual and Recurrent Glioblastoma with Deep Learning and multishell Diffusion MRI. *Neuro-Oncology Advances*. vdaf219, https://doi.org/10.1093/noajnl/vdaf219 (2025).
12. Hoebel, K. V. *et al.* Expert-centered Evaluation of Deep Learning Algorithms for Brain Tumor Segmentation. *Radiol Artif Intell.* **6**(1), e220231, https://doi.org/10.1148/ryai.220231 (2024).
13. Kickingereder, P. *et al.* Automated quantitative tumour response assessment of MRI in neuro-oncology with artificial neural networks: a multicentre, retrospective study. *Lancet Oncol.* **20**(5), 728–740, https://doi.org/10.1016/s1470-2045(19)30098-1 (2019).
14. Chang, K. *et al.* Automatic assessment of glioma burden: a deep learning algorithm for fully automated volumetric and bidimensional measurement. *Neuro-Oncol.* **21**(11), 1412–1422, https://doi.org/10.1093/neuonc/noz106 (2019).
15. Rudie, J. D. *et al.* Longitudinal Assessment of Posttreatment Diffuse Glioma Tissue Volumes with Three-dimensional Convolutional Neural Networks. *Radiology Artif Intell.* **4**(5), e210243, https://doi.org/10.1148/ryai.210243 (2022).
16. Lotan, E. *et al.* Development and Practical Implementation of a Deep Learning–Based Pipeline for Automated Pre- and Postoperative Glioma Segmentation. *Am J Neuroradiol.* **43**(1), 24–32, https://doi.org/10.3174/ajnr.a7363 (2021).
17. Ghaffari, M. *et al.* Automated post-operative brain tumour segmentation: A deep learning model based on transfer learning from pre-operative images. *Magn Reson Imaging.* **86**, 28–36, https://doi.org/10.1016/j.mri.2021.10.012 (2022).
18. Sørensen, P. J. *et al.* Evaluation of the HD-GLIO Deep Learning Algorithm for Brain Tumour Segmentation on Postoperative MRI. *Diagnostics.* **13**(3), 363, https://doi.org/10.3390/diagnostics13030363 (2023).
19. Vollmuth, P. *et al.* Artificial intelligence (AI)-based decision support improves reproducibility of tumor response assessment in neuro-oncology: An international multi-reader study. *Neuro-Oncol.* **25**(3), 533–543, https://doi.org/10.1093/neuonc/noac189 (2022).
20. Baig, S. *et al.* Segmentation of Pre- and Post-Treatment Diffuse Glioma Tissue Subregions Including Resection Cavities. *Neuro-Oncol Adv.* **6**(1), vdae140, https://doi.org/10.1093/noajnl/vdae140 (2024).
21. Fields, B. K. K. *et al.* The University of California San Francisco Adult Longitudinal Post-Treatment Diffuse Glioma MRI Dataset. *Radiol: Artif Intell.* **6**(4), e230182, https://doi.org/10.1148/ryai.230182 (2024).
22. Cepeda, S. *et al.* The Río Hortega University Hospital Glioblastoma dataset: A comprehensive collection of preoperative, early postoperative and recurrence MRI scans (RHUH-GBM). *Data Brief.* **50**, 109617, https://doi.org/10.1016/j.dib.2023.109617 (2023).
23. de Verdier, M. C. *et al.* The 2024 Brain Tumor Segmentation (BraTS) Challenge: Glioma Segmentation on Post-treatment MRI. *arXiv*. (2024).
24. Suter, Y. *et al.* The LUMIERE dataset: Longitudinal Glioblastoma MRI with expert RANO evaluation. *Sci Data.* **9**(1), 768, https://doi.org/10.1038/s41597-022-01881-7 (2022).
25. White, N. S., Leergaard, T. B., D'Arceuil, H., Bjaalie, J. G. & Dale, A. M. Probing tissue microstructure with restriction spectrum imaging: Histological and theoretical validation. *Hum Brain Mapp.* **34**(2), 327–346, https://doi.org/10.1002/hbm.21454 (2013).

26. Peruzzo, D., Bertoldo, A., Zanderigo, F. & Cobelli, C. Automatic selection of arterial input function on dynamic contrast-enhanced MR images. *Comput Meth Prog Bio.* **104**(3), e148–e157, https://doi.org/10.1016/j.cmpb.2011.02.012 (2011).
27. Boxerman, J. L., Schmainda, K. M. & Weisskoff, R. M. Relative cerebral blood volume maps corrected for contrast agent extravasation significantly correlate with glioma tumor grade, whereas uncorrected maps do not. *Ajnr Am J Neuroradiol.* **27**(4), 859–867 (2006).
28. Mazziotta, J. *et al*. A probabilistic atlas and reference system for the human brain: International Consortium for Brain Mapping (ICBM). *Philos Trans R Soc Lond Ser B: Biol Sci.* **356**(1412), 1293–1322, https://doi.org/10.1098/rstb.2001.0915 (2001).
29. Menze, B. H. *et al*. The Multimodal Brain Tumor Image Segmentation Benchmark (BRATS). *IEEE Trans Me d Imaging.* **34**(10), 1993–2024, https://doi.org/10.1109/tmi.2014.2377694 (2015).
30. Gagnon, L. *et al*. The University of California San Diego annotated post-treatment high-grade glioma multimodal MRI dataset. *The Cancer Imaging Archive*. https://doi.org/10.7937/fwv2-dt74 (2024).
31. HM, E. *et al*. MGMT Gene Silencing and Benefit from Temozolomide in Glioblastoma. *New Engl J Med.* **352**(10), 997–1003, https://doi.org/10.1056/nejmoa043331 (2005).
32. Bleeker, F. E., Molenaar, R. J. & Leenstra, S. Recent advances in the molecular understanding of glioblastoma. *J Neuro-Oncol.* **108**(1), 11–27, https://doi.org/10.1007/s11060-011-0793-0 (2012).

Acknowledgements

This work was supported by FRQS Junior 1, NSERC Discovery and RSNA seed grants (L.G.) and by a NIH-SBIR 1R44NS120796-01A1 grant (J.D.R.).

Author contributions

L.G., J.D.R. Guarantors of integrity of entire study; All authors contributed to study concepts/study design or data acquisition or data analysis/interpretation; All authors contributed to manuscript drafting or manuscript revision for important intellectual content; All authors contributed to approval of final version of submitted manuscript.

Competing interests

L.G. No relevant relationships. D.G. No relevant relationships. U.N. No relevant relationships. M.C.V No relevant relationships. R. S. No relevant relationships. G.M. No relevant relationships. N.W. National Institutes of Health Small Business Innovation Research grant no. 4R44NS120796. V.G. No relevant relation- ships. C.R.M. Grants from the National Institutes of Health/National Institute of Neu- rological Disorders and Stroke; consulting fees from Neurona. T.B. No relevant relation- ships. C.C. No relevant relationships. T.M.S. Grant to institution from GE HealthCare; consulting fees from GE HealthCare and CorTechs Labs; honoraria for educational events from GE HealthCare, Janssen, and Varian Medical Systems; support for travel/ attending meetings from Janssen and Varian Medical Systems; scientific advisory board member for CorTechs Labs; stock options in CorTechs Labs. J.H.G. No relevant relationships. S.K. Stock in CorTechs. J.D.S. No relevant relationships. D.P. No relevant relationships. K.M.S. Grants to institution from the Na-tional Institutes of Health/National Cancer Institute (R01CA082500, R01CA255123, and U01CA176110); board membership for Prism Clinical Imaging (nonpaid); stock ownership interest in IQ AI and Prism Clinical Imaging; salary for author and author's spouse from Imaging Biometrics. N.F. Participation on a data safety monitoring board or advisory board for CorTechs. A.M.D. Grants from the National Institutes of Health (U24DA041123, R01AG076838, U24DA055330, and OT2HL161847); funding through a research agreement with GE HealthCare; member of the scientific advisory board for CorTechs Labs, Human Longevity, and the Mohn Medical Imaging and Visualization Centre; founder of and holds equity in CorTechs Labs. J.D.R. Small Business Innovation Research/Small Business Technology Transfer grant 1R44NS120796-01A1 awarded to Cortechs.ai; American Society of Neuroradiology Research Grant in Artificial Intelligence; consulting fees from Cortechs.ai; medical advisory board member for Cortechs.ai and Subtle Medical; associate editor at *Radiology: Artificial Intelligence*; stock/stock options in Cortechs.ai and Subtle Medical.

Additional information

Correspondence and requests for materials should be addressed to L.G.

Reprints and permissions information is available at www.nature.com/reprints.

Publisher's note Springer Nature remains neutral with regard to jurisdictional claims in published maps and institutional affiliations.

Open Access This article is licensed under a Creative Commons Attribution 4.0 International License, which permits use, sharing, adaptation, distribution and reproduction in any medium or format, as long as you give appropriate credit to the original author(s) and the source, provide a link to the Creative Commons licence, and indicate if changes were made. The images or other third party material in this article are included in the article's Creative Commons licence, unless indicated otherwise in a credit line to the material. If material is not included in the article's Creative Commons licence and your intended use is not permitted by statutory regulation or exceeds the permitted use, you will need to obtain permission directly from the copyright holder. To view a copy of this licence, visit http://creativecommons.org/licenses/by/4.0/.

© The Author(s) 2026